ARTICLE

Tuning the drug multimodal release through a co-assembly strategy based on magnetic gels

Received 00th January 20xx,
Accepted 00th January 20xx

DOI: 10.1039/x0xx00000x

Sérgio R. S. Veloso[a], Ecem Tiryaki[b], Carlos Spuch[c], Loic Hilliou[d], C. O. Amorim[e], V. S. Amaral[e], Paulo J. G. Coutinho[a], Paula M. T. Ferreira[f], Verónica Salgueiriño[b,g,*], Miguel A. Correa-Duarte[g,*], and Elisabete M. S. Castanheira[a,*]

Self-assembled short peptide-based gels are highly promising drug delivery systems. However, implementing a stimulus often requires screening different structures to obtain gels with suitable properties, and drugs might not be well encapsulated and/or cause undesirable effects on the gel's properties. To overcome this challenge, a new design approach is presented to modulate the release of doxorubicin as model chemotherapeutic drug through the interplay of (di)phenylalanine-coated magnetic nanoparticles, PEGylated liposomes and doxorubicin co-assembly in dehydropeptide-based gels. The composites enable an enhancement of the gelation kinetics in a concentration-dependent manner, mainly through the use of PEGylated liposomes. The effect of the co-assembly of phenylalanine-coated nanoparticles with the hydrogel display a concentration and size dependence. Finally, the integration of liposomes as doxorubicin storage units and of nanoparticle as composites that co-assemble with the gel matrix enable the tuneability of both passive and active doxorubicin release through a thermal, low-frequency alternating magnetic field-based trigger. In addition to the modulation of the gel properties, the functionalization with (di)phenylalanine improves the cytocompatibility of the nanoparticles. Hereby, this work paves ways for the development of peptide-based supramolecular systems for on-demand and controlled release of drugs.

Introduction

Current chemotherapeutic strategies face major challenges associated with the lack of specificity and therapeutic effectiveness [1]. By using drug delivery systems, it is possible to minimize the side effects, increase therapeutic potential, and attain both spatial and temporal control [2,3]. Particularly, the combination of hydrogels and thermoresponsive liposomes is highly promising as the combination of the transport resistance by both materials (lipid bilayer and hydrogel matrix) endows a material with prolonged and controlled drug release, averts the initial burst release, and enables the localized and thermally triggered release of the payload [3,4]. Further combination with magnetic nanoparticles into magnetic liposome-hydrogel composites (magnetolipogels) surpass the difficulty of balancing a low permeability and high drug release efficiency, besides enabling the control of system's behaviour through an externally applied magnetic field [5]. In addition, the nanoparticles' generated heat (magnetic hyperthermia) synergistically enhances the drug's distribution [6] and therefore efficacy [7,8].

Despite the majority of the reported systems being based on polymeric hydrogels [5,9], the supramolecular are more advantageous owing to the low bioaccumulation, low-cost of manufacturing, structural versatility, easy metabolism and biocompatibility [10,11].

Recently, we demonstrated that the encapsulation of curcumin-loaded magnetoliposomes in peptide-based hydrogels led to a drug partition between both systems and displayed slower drug release than the neat hydrogel [12]. Regarding the peptide supramolecular magnetic gels, significant breakthroughs have been reported in the fabrication and associated properties. For instance, in the pioneer work by Yang et al. [13], nanoparticles functionalized with dopamine N-capped diphenylalanine were demonstrated to co-assemble with 2-Naph-L-Phe-L-Phe-OH hydrogelator during gelation, thus integrating hydrogel fibres.

[a] Physics Centre of Minho and Porto Universities (CF-UM-UP), University of Minho, Campus de Gualtar, 4710-057 Braga, Portugal.
[b] Departamento de Física Aplicada, Universidade de Vigo, 36310 Vigo, Spain.
[c] Translational Neuroscience Research Group, Galicia Sur Health Research Institute, CIBERSAM, Hospital Álvaro Cunqueiro, Bloque Técnico, Planta 2, Sala de Investigación, Estrada Clara Campoamor, 341, 36212 Vigo, Spain.
[d] Institute for Polymers and Composites, Department of Polymer Engineering, University of Minho, Campus de Azurém, 4800-058 Guimarães, Portugal.
[e] Physics Department and CICECO, University of Aveiro, Campus de Santiago, 3810-193 Aveiro, Portugal.
[f] Centro de Química (CQUM), University of Minho, Campus de Gualtar, 4710-057 Braga, Portugal.
[g] CINBIO, Universidad de Vigo, 36310 Vigo, Spain.
*Corresponding authors: vsalgue@uvigo.es; macorrea@uvigo.es; ecoutinho@fisica.uminho.pt

Electronic Supplementary Information (ESI) available: Experimental Synthesis of the hydrogelator; Molecular dynamics results; Self-assembly parameters; Combination of liposomes and hydrogels; Development and characterization of magnetic nanoparticles; X-ray diffraction parameters; Raman analysis of (calcium-doped) manganese ferrite; Functionalized nanoparticles magnetic properties; Fabrication of magnetic gels; Passive and active doxorubicin release; Cytotoxicity results. See DOI: 10.1039/x0xx00000x

Similarly, Das et al. [14] reported the co-assembly of polydopamine spheres coated with iron oxide nanoparticles with the peptide diphenylalanine to form magnetic hydrogels. As a means to simplify the fabrication, Nowak et al. [15] demonstrated that the addition of aspartic acid to the C-terminal enabled coordination of nanoparticles' metal ions, which enabled the co-assembly with the nanoparticles working as a cross-linker that increased gel's elasticity. An anisotropic change of elasticity was recently reported by Contreras-Montoya et al. [16] in anisotropic gels bearing PEGylated nanoparticles covered with Fmoc-L-Phe-L-Phe-OH. However, a decrease of peptide gels' elasticity can also occur as reported for gels bearing polyacrylic acid-coated nanoparticles [17], bare core@shell magnetic@plasmonic nanoparticles (plasmonic magnetogels) [18], or stabilized with citrate or lipids [19].

A major advantage of supramolecular peptide hydrogels is the improved control in drug delivery as the payload can participate/co-assemble in the hydrogel network formation. This property was demonstrated for different small molecules including ciprofloxacin, rhodamine B, naproxen and ketoprofen [20,21], and also evidenced in works reported by our group for curcumin and doxorubicin [10,18,19,22]. Particularly, doxorubicin, one of the most commonly used chemotherapeutic drugs for different cancers that has associated various side effects, was demonstrated by Xue et al. [23] to co-assemble with peptide-based gels as a cross-linker, which increases the inter-fibre interactions. This strategy, besides increasing the gel's elasticity, also induced a slower drug release as the concentration of doxorubicin was increased. However, in order to achieve efficient systems for on-demand and controlled release of drugs that can provide a high specificity and therapeutic effectiveness further synthetic developments need to be performed.

Hereby, we undertook a systematic and multi-targeted approach to improve drug delivery systems based in peptide-based gels towards supramolecular magnetic lipogels. Initially, we synthesized and characterized a new hydrogelator bearing a dehydroamino acid, 2-Naph-L-Phe-*Z*-ΔPhe-OH (compound 1), to provide proteolytical stability and favour self-assembly. Secondly, to improve the inherent biocompatibility of nanoparticles, manganese ferrites doped with Ca^{2+} or Mg^{2+} were synthesised through co-precipitation and explored as a means to reduce the use of transition metals while seeking for good magnetic properties [24,25]. The particles were coupled with phenylalanine and diphenylalanine as functional groups after previous addition of (3-aminopropyl)triethoxysilane (APTES), not only to assess the role of aromatic rings and cationic amine group as a novel strategy in co-assembly, but also to improve the biocompatibility [26,27]. Various techniques were used to confirm the functionalization, including UV-Vis spectroscopy, DLS and Raman spectroscopy. Further, the particles iron content, as well as the structural and magnetic propertie,s were also assessed and characterized through spectroscopic techniques, STEM, XRD and SQUID. The interaction of dehydropeptide-based hydrogels with liposomes was assessed and the systems were screened so to optimize the controlled and triggered release of doxorubicin. In Scheme 1, a summary of the fabrication of the system is included. Further, biological assays were carried out to assess the cytocompatibility of the developed strategy.

The present work not only proposes the use of functionalized particles and the co-assembly of different composites to modulate the properties of supramolecular gels, but includes the control over both the active and passive drug release. In this way, compared to previous reports with supramolecular peptide-based gels [5,12-19], the system averts the use of specific preparation protocols and/or introduction of chemical changes in the gelator molecules that might lead to undesired effects on the gel's properties. In addition, the system design broadens the array of possible gelators as it surpasses the limitation of the need for the commonly used thermoresponsive gels [28], as liposomes are used as stimuli-responsive storage units, and increases the amount of drug that can be loaded compared to (magnetic) liposomes alone, while ensuring a sustained release [5,12]. Therefore, as far as we know, this is the first work to unravel fundamental aspects of supramolecular dipeptide-based magnetic lipogels, while assessing a novel design strategy for co-assembly of hydrogelator and particles. This strategy provides an optimized drug delivery system for chemotherapeutic drugs, enabling temporal and spatial on-demand and prolonged drug release through magnetic stimulus, which makes use of liposomes as drug storage units.

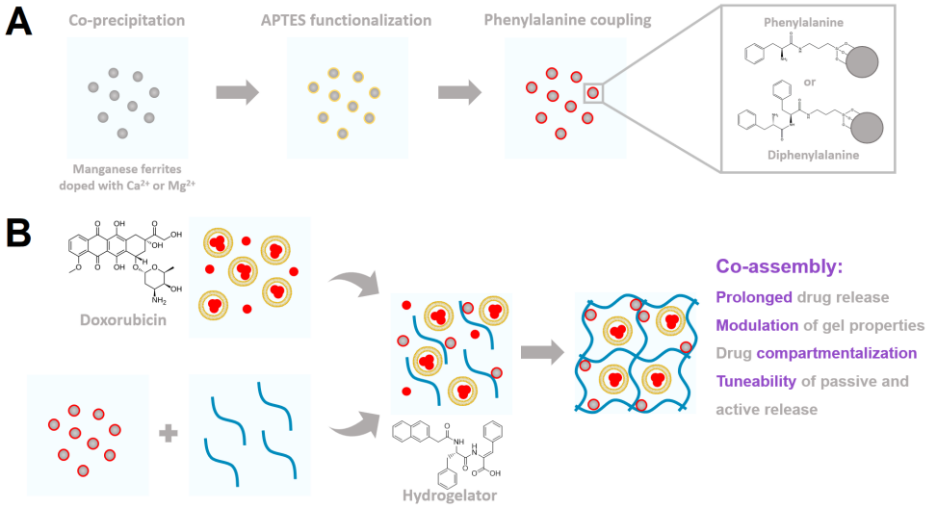

Scheme 1. Schematic summary of the fabricated system. (A) Initially, various manganese ferrites doped with Ca^{2+} and Mg^{2+} were screened based on the expected magnetic properties. The particles were then functionalized with APTES and posteriously coupled with phenylalanine to a protocol adapted from the solid phase peptide synthesis strategy. To obtain diphenylalanine, the coupling reaction was repeated on the phenylalanine coated nanoparticles. (B) The nanoparticles were combined with the gelator solution, following the addition of a PEGylated liposomes solution containing both encapsulated and free doxorubicin. The resulting system (magnetic liposome-hydrogel) stemming from the co-assembly of the different components (doxorubicin, liposomes, nanoparticles and the hydrogelator) can have the properties modulated by the co-assembled composites.

Results and discussion

Preparation of supramolecular lipogels

Synthesis of the dehydropeptide. The dehydrodipeptide *N*-capped with a 2-naphthalene acetyl group (2-Nph) was prepared using a conventional protocol in solution (see Scheme S1 in Supplementary Information). Briefly, the coupling reactions were performed using either *N,N'*-dicyclohexylcarbodiimide (DCC)/1-hydroxybenzotriazole (HOBt) as the coupling agent. Dehydration of the β-hydroxydipeptide was accomplished by its reaction with di-tert-butyl dicarbonate (Boc_2O) in the presence of 4-dimethylaminopyridine (DMAP), followed by treatment with *N,N,N',N'*-tetramethylguadinine (TMG) [29]. Compound 1 was obtained after basic cleavage of the methyl ester *N*-naphthalene acetyl protected dehydrodipeptide (see Figure S1 Supplementary Information).

(Di)Phenylalanine interaction with hydrogelator aggregates. Molecular dynamics was used to evaluate the potential interaction of (di)phenylalanine with the dehydropeptides aggregates. The increase of the root-mean-square deviation values (see Figure S2 in Supplementary Information) suggests the occurrence of aggregation, and its fluctuation is an indication of different aggregate conformations over time, which in general stabilizes after 40 ns. Visualization of the aggregation process snapshots (see Figure S3 of the Supplementary Information) reveals that dehydropeptides form aggregates during the 60 ns timescale, which is associated with the intermolecular π-π interactions between the *N*-capping group and the aromatic amino acids [30]. Further, the (di)phenylalanine residues also participate in the aggregation process.

The most representative clusters over the last 20 ns are displayed in Figure S4, which were detected through the single-linkage method with a RMSD cut-off of 1.4 nm. The dehydropeptides form a nucleus, while the added phenylalanine residues (Phe(R)) accumulate in the exterior and the diphenylalanine residues (Phe-Phe(R)) seem to integrate the nucleus. For instance, despite the average solvent exposed areas (SASAs) converging for similar values, the dehydropeptide's average SASA per residue (see Figure S5A,B in Supplementary Information) remains similar to the simulations in the presence of Phe(R), while it decreases in the presence of Phe-Phe(R). The radius of gyration (see figure S5C in Supplementary Information) also evidences the structure fluctuation, mainly when Phe(R) is added. Further, together with the decrease of the shape indicator parameter asphericity [31,32] (less elongated aggregates) (see figure S5D in Supplementary Information) in the presence of both Phe(R) and Phe-Phe(R), the abovementioned results suggest it to be a consequence of the adsorption of the added residue on the aggregates.

Hydrogel properties and self-assembly. Gels prepared through GdL addition to a basic solution (2 v/v% NaOH 1M) formed reversible gels with at least 0.4 wt% of hydrogelator and 0.3 wt% of GdL, which corresponds to a pH range from 6.9 to 8.3. However, an increase of GdL concentration to 0.4 wt% induced the formation of irreversible gels (see figure S6 in Supplementary Information). In addition, it was also possible to prepare gels through a heating-cooling cycle (heating up to 80 °C and cooling at room temperature) down to 0.2 wt% of hydrogel at pH 7.4 (see figure S7 in Supplementary Information).

Hydrogel's morphology. Fluorescence emission from the direct excitation (λ_{exc}=280 nm) of hydrogelator results in a sharp band around 360 nm and a broad band centered at 450 nm, associated with the monomer and aggregates formed through π-π stacking of the aromatic rings, respectively (see excitation in figure S8A-C in Supplementary Information) [10,18]. An increase of GdL or hydrogelator concentration induced a reduction of fluorescence emission as a consequence of the increased inner filter effect, as well as the formation of aggregates (quenching of the monomer emission). Further, both the emission from the monomer and aggregates (see figure S8D in Supplementary Information) is redshifted in gels prepared through GdL compared to the ones prepared from a heating-cooling cycle (around 350 nm), which evidences a different final structure according to the preparation method as characteristic of supramolecular hydrogels [33]. For instance, the gels prepared through GdL formed entangled fibers with an average cross-section of 21.76 ± 6.20 nm, while the heating-cooling cycle method resulted in helical fibers with an average cross-section of 24.39 ± 7.73 nm (see figures 1A,B and S9 in Supplementary Information).

Self-assembly kinetics. The kinetic assays further reveal the influence of the preparation method on the final structure (figure 1C,D), which was also observed in other dehydropeptides [10,19]. Here, the aggregates' shape changes during gelation and the high dependence of the final structure on the preparation conditions prevent the assessment of self-assembly processes through turbidity as reported in reference [19]. However, comparison with fluorescence kinetics assays suggest that even during self-assembly equilibrium, structural changes are occurring.

In general, gels reached equilibrium after 2 hours, a larger hydrogel-to-GdL ratio decreased the turbidity gelation rate, and gels prepared through a heating-cooling method are more turbid (see figure S10A,B in Supplementary Information), which suggests the presence of irregular aggregates. The decrease of the turbidity gelation rate with increasing gelator concentration (for same GdL concentration) can be associated with a slower formation of fibres. For instance, fitting of Saitô's model [34] to fluorescence kinetics revealed a general decrease of nucleation-to-elongation rate for larger hydrogelator-to-GdL ratio (see figure S10C,D in Supplementary Information). In addition, gels prepared at 0.4 wt% GdL display similar self-assembly (fluorescence) kinetics and fluorescence anisotropy values for increasing hydrogelator concentration (figure 1E).

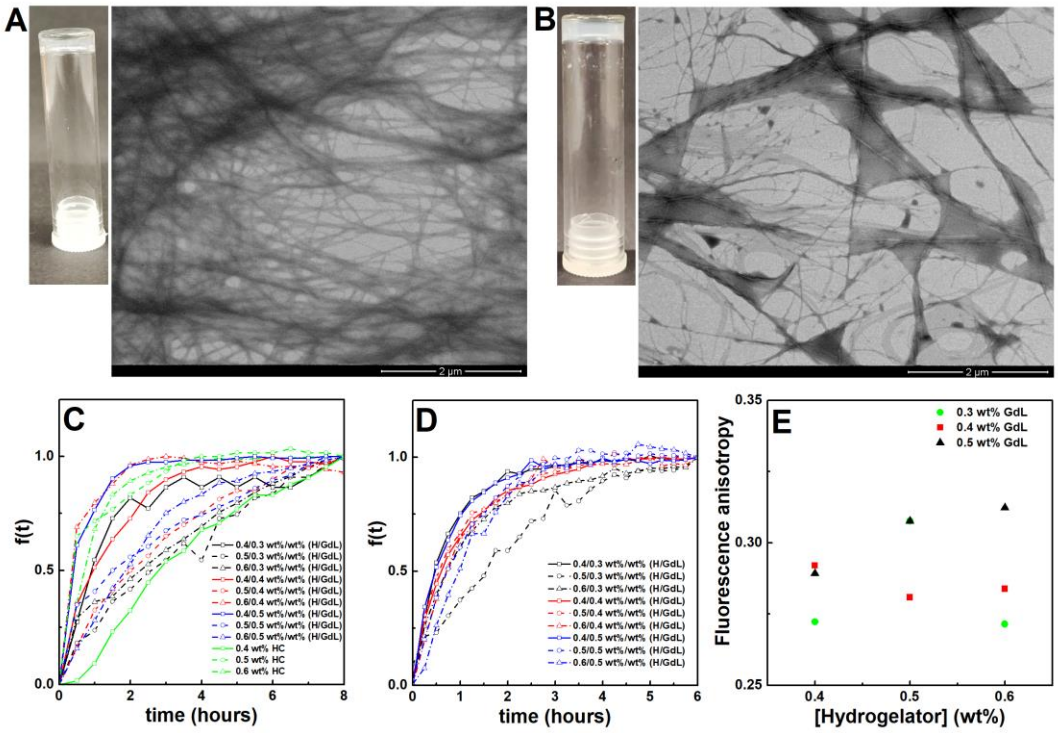

Figure 1. STEM images of hydrogels prepared at 0.5 wt% of hydrogelator through (A) the GdL (0.4 wt%) method and (B) heating-cooling cycle method (phosphate buffer pH=7.4). Images of gels are included. (C) Turbidity (absorbance masured at 500 nm) and (D) fluorescence emission (Nile Red, 2 µM, λ_{exc}=520 nm, λ_{em}=620 nm) kinetic profile dependence on hydrogelator and GdL concentration, in which f(t) stands for the aggregates faction (equation S3 defined in Supplementary Information). (E) Nile Red fluorescence anisotropy in gels at different GdL and hydrogelator concentrations.

Development of supramolecular liposome-hydrogel formulations. Various liposome formulations comprising DPPC, egg-PC, cholesterol, DOPG and DOPE were combined with hydrogels to assess changes in membrane microviscosity at increasing temperatures through fluorescence anisotropy of 1,6-Diphenyl-1,3,5-hexatriene (DPH) (see figure S11 in Supplementary Information) [35]. In all samples, the similar DPH fluorescence anisotropy at increasing temperatures suggests the occurrence of lipid-hydrogel interactions, which were also reported in other dehydropeptide supramolecular hydrogels [12,19]. Further, DPPC liposomes displayed close DPH anisotropy values in different hydrogel concentrations, while significant changes were observed in other formulations, which suggests the DPPC membranes to be stable under a larger range of peptide concentrations.

Gelation-induced liposome leakage. Liposome leakage has been reported to occur in formulations comprising liposomes and polymeric hydrogels [2,36]. In this regard, the DPPC liposomes were loaded with 5(6)-carboxyfluorescein (CF) and the effect of cholesterol and PEGylation was assessed as means to optimize the stability of the composite system (figure 2A). Despite cholesterol reducing membrane fluidity and hampering the release of CF in liposomes, the leakage from DPPC:Ch liposomes in gels was higher or comparable to the release from heat-triggered liposomes. The presence of PEG (5 mol%), besides reducing the leakage from gels, also displayed higher triggered release from the gel compared to all the other systems.

Implications of liposomes in self-assembly kinetics. The effect of DPPC:PEG liposomes over gelation was further studied in gels (0.4 wt% GdL, 0.5 wt% hydrogelator) loaded with Nile Red (see figure S11E in Supplementary Information). The increasing liposome content led to a decrease of both the nucleation rate and the average microviscosity (above 0.25 mM of liposome content) of the Nile Red microenvironment (see figure S11F,G). In addition, a blue shift and increasing fluorescence emission of Nile Red was obtained after gelation with the incremental liposome content, potentially associated with more hydrophobic cavities made available to which Nile Red localizes (see figure S11H in Supplementary Information).

Lipogels as doxorubicin carriers. PEGylated liposomes loaded with doxorubicin were incorporated in the gels, which led to an attenuated fluorescence emission associated with the inner filter effect (figure 2B). The DPPC:Ch:PEG 17:2:1 (EE(%) ± SD(%) = 81.6 ± 5.5 % for 20 μM) displayed a lower fluorescence emission than DPPC:PEG 19:1 (EE(%) ± SD(%) = 83.1 ± 3.2 % for 20 μM) liposomes in the gels, suggesting a higher leakage from the latter during the gelation as also supported by the close similarity with the emission from the neat hydrogels. Further, despite that the cholesterol containing liposomes displayed smaller size and zeta-potential, both lipogel converged to similar final doxorubicin fluorescence anisotropy, which was also observed for previously reported formulations (see table S1 in Supplementary Information) [9]. Such convergence suggests the occurrence of lipid-fiber interactions as also evidenced by the existence of large nucleation points in lipogels (not observed in hydrogels) that resemble liposomes embedded in the hydrogel matrix (figure 2C).

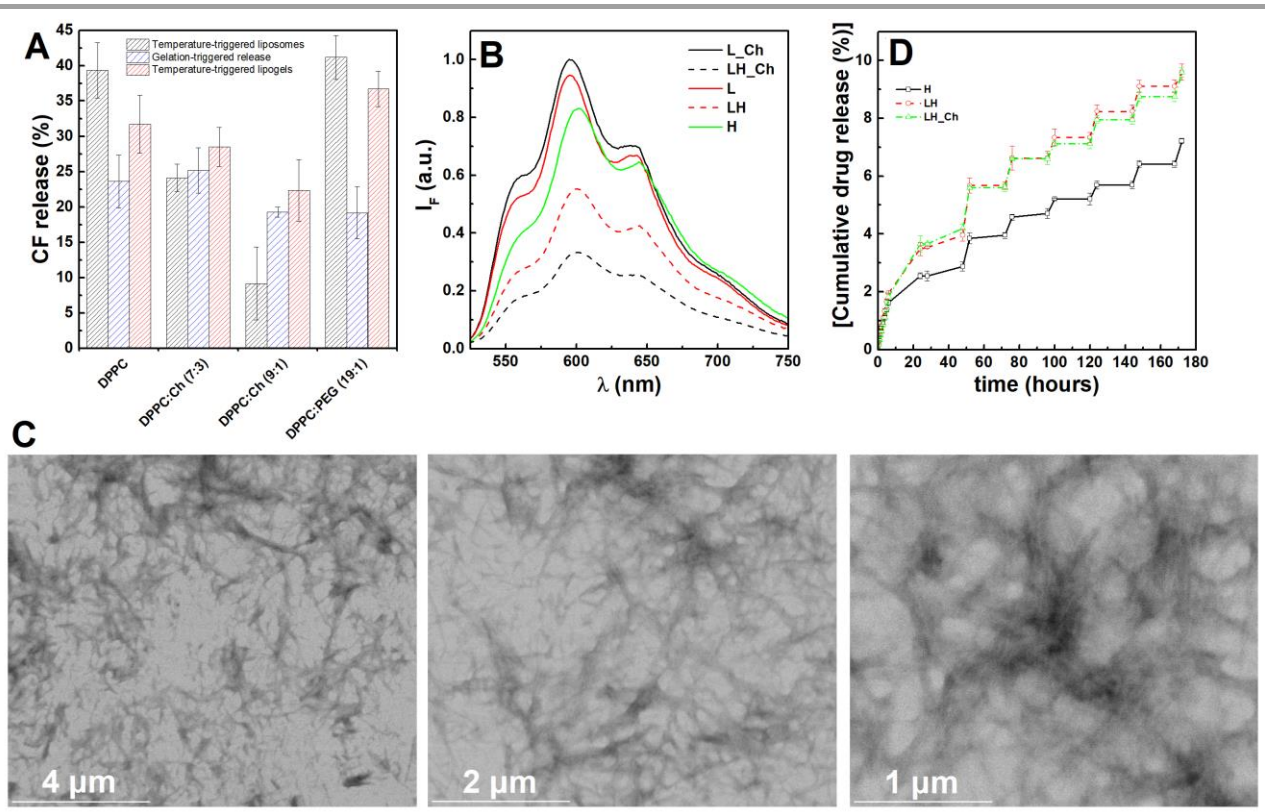

Figure 2. (A) Release percentage of 5(6)-carboxyfluorescein loaded in liposomes of different composition to pH 7.4 phosphate buffer: after heating of liposomes for 30 min at 45 °C (HL); from hydrogel (0.5 wt%) bearing liposomes after 3 hours (+24 h of gelation) (G); and after heating of the combined hydrogel-liposome system (HG) for 30 min at 45 °C. (B) Fluorescence spectra of directly-excited doxorubicin (10 μM, λ_{exc}=480 nm). (C) STEM images of a lipogel bearing DPPC:Ch:PEG 17:2:1 liposomes (0.5 mM) prepared at 0.5 wt% of hydrogelator. (D) Cumulative doxorubicin release from the hydrogel and lipogels containing DPPC:Ch:PEG 17:2:1 or DPPC:PEG 19:1. Each cycle of heating (45 °C) was carried out for 1 h with an interval of 24 h and the first cycle was initiated after 48 h of passive release. Legend: L_Ch: DPPC:Ch:PEG

17:2:1 liposomes; LH_Ch: Lipogel with DPPC:Ch:PEG 17:2:1 liposomes; L: DPPC:PEG 19:1 liposomes; LH: Lipogel with DPPC:PEG 19:1 liposomes; H: hydrogel.

Influence of doxorubicin encapsulation in gels drug release. No major difference was observed between both lipogel formulations (with and without cholesterol) during doxorubicin passive and active release with a heating stimulus (figure 2D). The larger passive release from lipogels than hydrogels can be associated with a decrease of free doxorubicin in the gel phase, and consequently a diminished hydrogel-doxorubicin co-assembly [23]. Besides that, the triggered release was larger in both lipogels compared with the neat hydrogel, and decreased with each cycle (see figure S12A in Supplementary Information). The subjection of the gels to a larger contribution from erosion led to an increased release in all samples, which remained larger for the lipogels (see figure S12B in Supplementary Information).

Preparation of supramolecular magnetic lipogels

Synthesis of the magnetic core. The synthesis of ferrites doped with calcium, magnesium and manganese was attained with the aim of establishing a convenient compromise of suitable magnetic properties associated to the heat delivery ability required and decreased inherent toxicity [24,25]. For instance, while doping of manganese ferrites with calcium afforded high saturation magnetization (figure S13A in Supplementary Information), doping with magnesium resulted in a decrease in this parameter, but with the benefit in both cases of strongly reducing the iron content (see figure S13B and table S2 in Supplementary Information). Analysis of the XRD profiles (figure S14A,B) revealed that the doping cation influenced the final size, not only of the lattice unit but also of the crystalline domain in the nanoparticles, for the same reaction conditions. An average crystallite size of 9.3 nm and 4.7 nm was obtained for the neat and calcium-doped manganese ferrites, respectively (see table S3 for detailed analysis in Supplementary Information). Confirmation of the manganese and calcium doping was obtained through Raman spectroscopy (see analysis and figure S15 in Supplementary Information), offering spectra that displayed bands and contributions characteristic of (metal-doped) manganese ferrites [37,38]. Regarding the addition of APTES, the profiles only displayed a slight decrease of intensity and remained with the unchanged characteristic diffraction peaks of ferrites, suggesting an unaffected crystalline structure of the magnetic nucleus. Further, the final size is similar to the neat nanoparticles (figure 3A,B and size histogram in figure S14C,D), with the manganese ferrites (11.53 ± 4.13 nm) being larger than the calcium-doped (7.03 ± 2.10 nm).

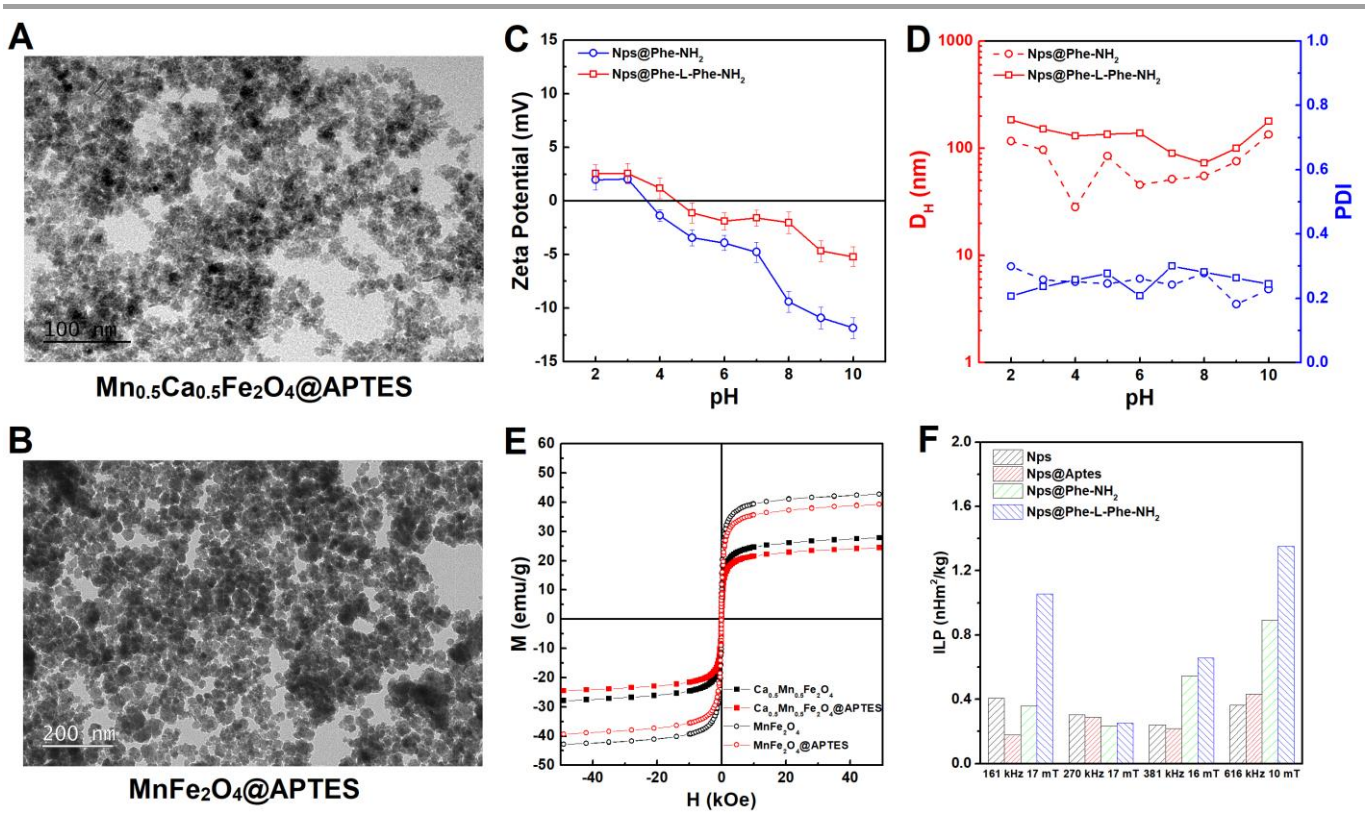

Figure 3. (A,B) Transmission electron microscopy image of the APTES-coated magnetic nanoparticles. (C) Zeta potential dependence on pH for calcium-doped manganese ferrites functionalized with phenylalanine or diphenylalanine. (D) Hydrodynamic size (D_H) obtained from number distribution and polydispersity index (PDI) of the functionalized nanoparticles. (E) Magnetization hysteresis loops of APTES coated (calcium-doped) manganese ferrite nanoparticles measured at room temperature (T=300 K). (F) Intrinsic loss power (ILP) calculated from the temperature variation over time of functionalized calcium-doped manganese ferrite nanoparticles in water (1 mg/mL) under different magnetic field strengths and frequencies.

Functionalization of magnetic nanoparticles. Raman spectroscopy was employed to evidence the successful functionalization of the magnetic nanoparticles with phenylalanine (Nps@Phe-NH_2) or diphenylalanine (Nps@Phe-L-Phe-NH_2) *N*-deprotected. Figure S16A (in the Supplementary Information) includes the Raman spectra in the 1100-1800 cm^{-1} range, in which the modes of vibration displayed can be associated to the phenylalanine functional groups [39-42]. The zeta potential profiles of the functionalized nanoparticles displayed a shift of the isoelectric point for larger pH after coupling of the second phenylalanine residue, besides lesser charged particles in the pH range 5-8 that lead to a larger hydrodynamic size (figure 3C,D). Thus, these results further confirm the functionalization, as the addition of cationic amine groups reduces the negative charge of the particles, while the addition of phenylalanine residues results in a larger organic shell. The sudden zeta potential change around pH 7-8 and pH 8-9 for Nps@Phe-NH_2 and Nps@Phe-L-Phe-NH_2, respectively, can be associated with the residues undergoing an ionization state transition from positively charged to neutral (apparent pK_a) at the interface of the material. The inflection points occur at lower pH values than the pK_a of phenylalanine NH_2 moiety in aqueous solution, which is characteristic of surface amino groups as also reported for APTES in a silicon surface that displayed an apparent pK_a of ≈7.6 value (compared to 10.6 in bulk solution) [43].
While the APTES functionalization of the nanoparticles implied a slight decrease of the saturation magnetization (figure 3E; likely associated to some oxidation at the surface), the coercivity remained unaltered. Accordingly, the intrinsic loss power values (ILP $\propto M_s^2$, also designated as SAR – specific absorption rate) were just slightly affected [44], keeping therefore the heating efficiencies of the APTES-coated nanoparticles. On the other hand, changes of the ILP values were registered for further functionalization of the magnetic nanoparticles with (di)phenylalanine (figure 3F and see manganese ferrite ILP values in figure S16C), though besides the functionalization and consequent changes at the surface of the nanoparticles, these changes should be also correlated to the different values of field strength and frequencies employed [45,46].

Fabrication of supramolecular magnetic gels. The combination of (di)phenylalanine stabilized nanoparticles with the hydrogels enabled the preparation of gels at high composite content (up to 0.8 wt%) for the same hydrogelator mass content (0.5 wt%). Remarkably, at high nanoparticle concentration, gels could support their own weight a day after a mechanical agitation (figure 4), which was not possible at low nanoparticle concentration. The same effect was obtained with simple APTES coated nanoparticles (see figure S17 in Supplementary Information). Transmission electron microscopy of magnetic gels (0.1 wt% of nanoparticle content) reveals the existence of the nanoparticles, as well as aggregates, distributed across the hydrogel matrix and close to the gel fibres in both magnetic gels containing functionalized nanoparticles.

The co-assembly of the nanoparticles with the hydrogel fibres was also evidenced in the early stages of the self-assembly kinetics (see figure S18 in Supplementary Information). Similar to the liposomes, the addition of nanoparticles enhanced the elongation rate in detriment of the nucleation. In addition, the Nile Red localizes in an environment with incremental reduction of microviscosity and increased polarity with the increase of nanoparticle content. This effect has also been observed in other magnetic gels, which were loaded with citrate- or lipid-stabilized nanoparticles [19].

Magnetic and mechanical properties of supramolecular magnetic lipogels

Tuneability of gels mechanical properties. The mechanical spectra of the hydrogels over time (figure 4C) evidenced a decrease of the lag time upon addition of nanoparticles, besides a convergence of the storage modulus (G') independent of the functionalization group ((di)phenylalanine) for the same particle size. In addition, regarding these two parameters, the use of the larger manganese ferrite nanoparticles (~ 12 nm) resulted in smaller reduction of the storage modulus while displaying similar lag time to the smaller calcium-doped manganese ferrites (~ 7 nm) for the same functionalization group (phenylalanine). However, as the phenylalanine-coated manganese ferrites content was reduced to 0.05 wt% the mechanical profiles approached the ones of the smaller particles (see figure S19A,B,C in Supplementary Information). In the opposite trend, the increase of the particle content to 0.2 wt% clearly demonstrated that a higher particle concentration reduces the lag time (faster gelation). The shorter gelation lag time in the presence of composites has also been reported in other gels [47]. In accordance with the TEM images, the nanoparticles distributed across the hydrogel matrix and close to the fibres might work as fillers (or cross-linkers) that reduce the required volume for the fibres to span the entire solution and thus achieve a gel state. The frequency sweeps (figure 4D) further confirm the strong solid-like nature of the gels as the G' is nearly frequency independent and a magnitude 100× larger than the loss modulus (G''). Besides, G'' strongly increased at larger frequencies as the dissipation of deformation energy as heat (the viscous behaviour) becomes more prominent. The results of the performed large amplitude oscillatory shear strain sweeps (LAOS) confirm a similar behaviour for the nanoparticles functionalized with (di)phenylalanine and same ferrite nucleus (figure 4E). All gels display a G' and G'' hardening at a critical strain characteristic of type IV materials [48], which is shifted for larger amplitudes in the magnetic gels and is less intense for the gels with smaller particles. These suggest the existence of strong intermolecular interaction between hydrophobic groups that can create shear-induced structures, including the destruction and reformation of microstructures [48,49].

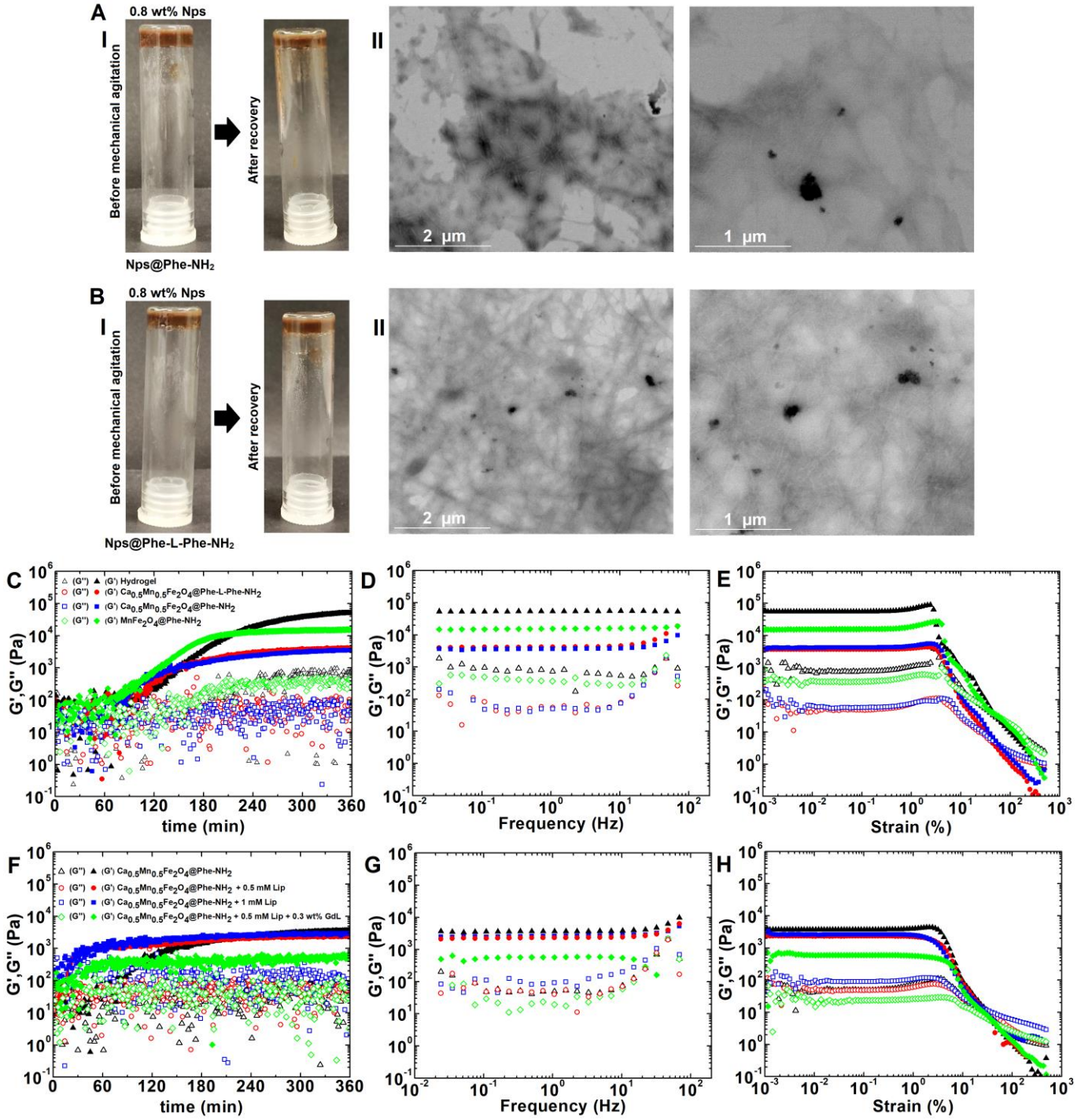

Figure 4. (AI, BI) Images of magnetic gels at high nanoparticle content (0.8 wt%) before and after breakage, and (AII, BII) the transmission electron microscopy images at lower content (0.1 wt%) of nanoparticles functionalized with (A) phenylalanine and (B) diphenylalanine. The gels we prepared with 0.5 wt% of hydrogelator, 0.4 wt% of GdL and particles with the calcium-doped manganese ferrites. (C) Shear storage G' (filled symbols) and loss G'' (empty symbols) modulus during the kinetic process of gelation, (D) frequency sweep and (E) strain sweep of hydrogel and magnetogels (0.5 wt% hydrogelator; 0.4 wt% GdL) bearing manganese or calcium-doped manganese ferrite nanoparticles coated with phenylalanine or diphenylalalnine at 0.1 wt%. (F) Shear storage G' (filled symbols) and loss G'' (empty symbols) modulus during the kinetic process of gelation, (G) frequency sweep and (H) strain sweep of magnetogel and magnetolipogels (0.5 wt% hydrogelator; 0.4

wt% GdL) bearing calcium-doped manganese ferrite nanoparticles coated with phenylalanine at 0.1 wt% and variable concentration of liposomes (Lip). Magnetolipogels prepared with 0.3 wt% of GdL are included.

Mechanical properties of magnetolipogels. The combination of magnetic gels with liposomes up to 1 mM strongly reduced the lag time from more than 1 hour to less than 20 minutes (figure 4F). The frequency sweep (figure 4G) displays a small decrease of the storage modulus, and an increase of the loss modulus for 1 mM of liposomes, i.e. the addition of liposomes seems to contribute for a reduction of the solid-like behaviour. Also, the G' hardening in the strain sweep profiles disappears (figure 4H), meaning the materials microstructure (now characteristic of a type III) might display a density decrease of the network's chains or a decrease of the intermolecular interactions forces causing the shear-induced structures.

Regarding the potential interest of a reversible gel on biomedical applications, the magnetolipogels were also fabricated with 0.3 wt% of GdL. This led to a slower kinetics, a decrease of the storage modulus, a higher dependence of the moduli on the frequency as characteristic of weaker gels and a strain dependency that approaches the behaviour of a type I material (shear thinning). Further, 3 hours after breakage, the gel recovered as a weaker solid (viscous behaviour at a lower frequency threshold) with a lower storage modulus, but the yielding (taken as the G' and G'' crossover) remained closely the same.

Perspective on the application of peptide-based magnetolipogels. Like previously developed dehydropeptide hydrogels, the gels (including magnetogels) here developed fall in the range of the native tissues and organs elastic modulus (e.g. skin, pancreas, spleen, glands, and muscles), ranging from 0.1 kPa (brain) to 1 MPa (cartilage) [50]. Such makes the systems adequate for biomedical applications, including tissue engineering and drug delivery. For instance, the former requires hydrogels with a stiffness closely matching the proposed extracellular matrix and that is sufficient to sustain cell growth, while the latter needs a stiffness that ensures the gel structure over the drug release time period [51].

The developed gels are comparable to previously reported dehydropeptides, such as Npx-L-Trp-*Z*-ΔPhe-OH hydrogel (stress modulus of 4 kPa at 0.4 wt% compound and 0.4 wt% GdL) [52], Npx-L-Phe-*Z*-ΔPhe-OH (1.7 kPa at 0.4 wt% pH=8 phosphate buffer) [30], Cbz-L-Phe-*Z*-ΔPhe-OH (187 kPa at 0.3 wt% compound and 0.5 wt% GdL) [10], diphenylalanine-based hydrogels [53], and also bis-dehydropeptide bolaamphiphiles [51]. Besides, the nanoparticles enabled a faster gelation and development of magnetic gels with high particle concentration (assessed up to 160 m/m%) without requiring extra GdL or hydrogelator as in previous magnetic gels [17,19].

The possibility of tuning the properties by varying the concentration of nanoparticles, liposomes and GdL enabled the development of reversible magnetic gels at 0.3 wt% of GdL (see figure S19D,E in Supplementary Information). Nonetheless, in addition to this possibility towards injectable self-healing gels, the fast gelation can also be explored as a means for fast in situ gelation. For example, the magnetogels (0.5 wt% compound and 0.4 wt% GdL) with phenylalanine-coated nanoparticles could be injected until 10 min post-induced gelation and provide a homogenous gel in less than 30 min (see figure S20 in Supplementary Information), in accordance with the rheology kinetic profiles.

Magnetolipogels as systems for magnetic hyperthermia. Overall, the incorporation of the nanoparticles in the hydrogels was associated with a slight decrease of the heating efficiency compared with the neat nanoparticles (see figure S21 in Supplementary Information). This has been observed for previously developed magnetogels [17,20], and can be explained taking into account the following effects: a) once the nanoparticles are embedded in the gels, some of the generated heat is employed for inducing local changes in the gel structure and not for increasing the temperature, b) the formation of particle aggregates during gelation (observed in the electron microscopy images) leads the nanoparticles to establish magnetic dipolar interactions, with the consequent deleterious effect in the heat efficiency [54], and d) the absence of Brownian motion and therefore of the Brownian relaxation, as having the nanoparticles trapped in the gels.

Drug release assays and *in vitro* experiments

Regarding the liposome formulation for the development of magnetolipogels, the DPPC:Ch:PEG 17:2:1 was preferred owing to the slight higher encapsulation efficiency, despite that the drug release profile was insignificantly different from the same formulation without cholesterol.

Passive release. Magnetolipogels and magnetogels were prepared with doxorubicin at 0.1 mM, and drug release was investigated at pH=7.4. The different magnetic nanoparticles were assessed to evaluate the influence of the particle coating in the drug release profiles, as well as the effect of the particle size ($Ca_{0.5}Mn_{0.5}Fe_2O_4$ < $MnFe_2O_4$).

The doxorubicin passive release profiles (first 24 h) in figure 5A clearly show that the magnetic composites influenced the drug release. Initially, all gels display a faster release rate, which is followed by a slower release phase in the later hours. This doxorubicin release profile has been observed for other gels based on carboxybenzyl-protected dehydropeptides [10,19]. Besides, the drug is not totally released after 3 days, which can be associated with the strong interactions stablished between doxorubicin and the hydrogel fibers. As previously discussed, doxorubicin has been reported to self-assemble with peptide-based gels as nanospherical assemblies that act as cross-linkers [23].

The combination of gels with nanoparticles hampered drugs release in all systems, including the magnetolipogels. A potential reason could be the nanoparticles acting as cross-linkers, but such is unclear

considering the elastic modulus decrease in the rheologic assays (despite the faster gelation kinetics). Another possibility is the nanoparticles working as fillers that occupy the mesh water pockets, which is in agreement with the diphenylalanine-coated nanoparticles (larger hydrodynamic size) inducing a stronger hampering of drug release than the phenylalanine-coated nanoparticles. Also, the larger manganese ferrite nanoparticles hampered more the release than the smaller calcium-doped particles. Further insight in the passive release is provided by fitting several mathematic models to the cumulative drug release profiles (see table S5 in Supplementary Information). In line with previous works with short peptide-based gels [10,19], the drug release is well described by the Gompertz and Korsmeyer-Peppas models (see Eqs. (S4) and (S5) in Supplementary Information). The latter model can be applied to systems of different geometries requiring that perfect sink conditions are maintained [55-57]. Such was ensured in the developed gels and drug release occurred only in the vertical direction (gels adhered the bottom of the vials). While the Gompertz model enables an empirical comparison of the release kinetics, the parameter *n* of the Korsmeyer-Peppas model provides information on the diffusion mechanism. The determined constants and parameters are presented in table S5 in Supplementary Information. In general, both models suggest that the release is hampered in the presence of nanoparticles (further reduces with concentration), but the (magneto)lipogels attained higher release rate and higher amount of drug release. Regarding the drug release mechanism, the low *n* values are characteristic of diffusion-controlled release mechanism, but analysis of the first 6 hours indicate the occurrence of diffusion and erosion drug release as observed for other gels loaded with doxorubicin [10,19], potentially associated with the induced erosion of the buffer replacement.

Active release. Temperature and low-frequency AMF were assessed as triggers for doxorubicin release during the slow regime of the drug release profiles (after 48h). The former trigger has been extensively studied in liposomes considering the possibility of stablishing a synergy with magnetic hyperthermia (provided by the magnetic nanoparticles) [58]. In this way, it was also assessed for the magnetolipogels as the nanoparticles were able to heat the entire gel volume through magnetic hyperthermia. The temperature increase is expected to induce a phase transition of the liposomes, which consequently leads to more doxorubicin being released from the liposomes to the hydrogel matrix that can diffuse out of the gel matrix, i.e. the liposomes work as storage pockets of doxorubicin. In this regard, and similarly to lipogels, the magnetolipogels display a strong initial thermally-triggered release compared to the magnetogels owing to the doxorubicin made available by the liposomes.

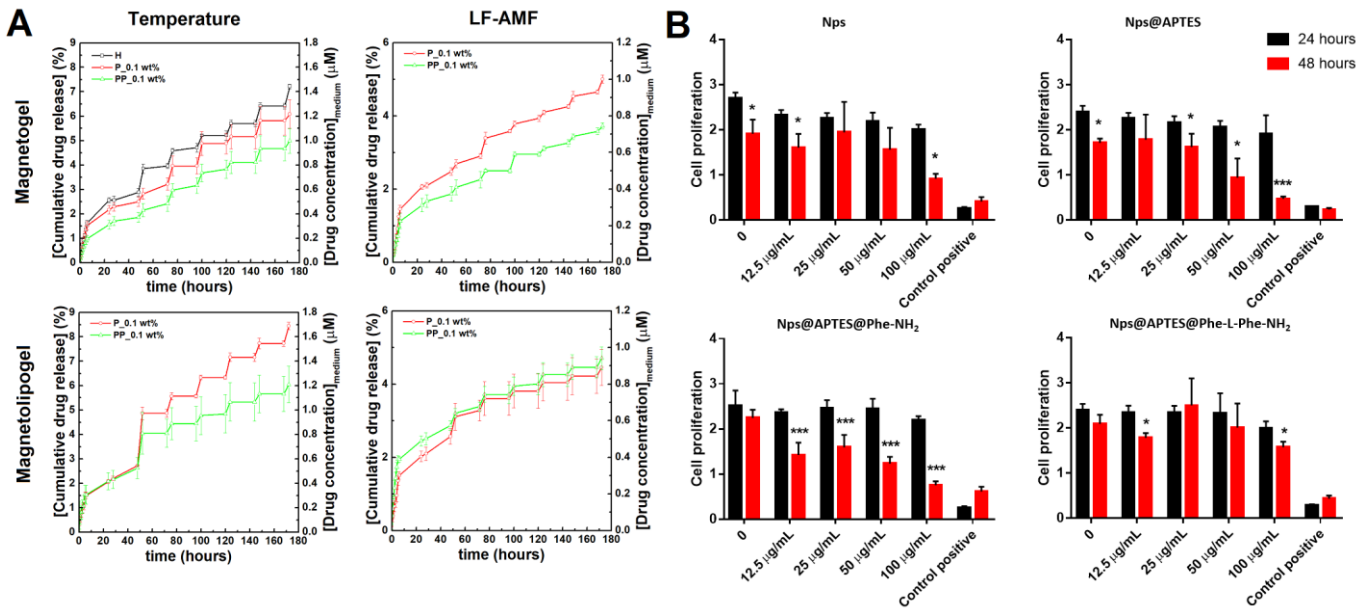

Figure 5. (A) Cumulative doxorubicin release from magneto(lipo)gels containing phenylalanine (P) and diphenylalanine (PP) functionalized calcium-doped manganese ferrite nanoparticles (0.1 wt%) to phosphate buffer pH=7.4. The gels were subjected either to a heating cycle (45 °C) carried out for 1 h with an interval of 24 h or a low-frequency magnetic field (LF-AMF) for 2 hours. The first cycle was initiated after 48 h of passive release. The concentration of doxorubicin in gels is 100 μM, and the maximum that can be accumulated in the medium is 20 μM (200 μL gel for 800 buffer medium). (B) In vitro cell proliferation assays of magnetic nanoparticles with the core of calcium-doped manganese ferrite (Nps) functionalized with APTES, phenylalanine and diphenylalanine performed with U373 MG human glioma cell line by the MTT assay. Data is represented as mean ± SD, and n = 12. *Denotes significant difference between sample and control groups ($p < 0.05$).

Alternatively, a low-frequency AMF can be used to induce doxorubicin release. These fields are safe, penetrate deep tissues and do not affect the surrounding organs and tissues [59]. The LF-AMF is commonly used in magnetoliposomes to induce drug release through the mechanical strain exerted by the particles on the membrane [59,60]. Here, the drug release can be enhanced

considering that the gel network confines the liposomes to a closer proximity of the nanoparticles, and that the latter are also associated with the hydrogel fibrils. The results demonstrate that the (di)phenylalanine coated nanoparticles attained similar drug release values in the magnetolipogels, while in the magnetogels the phenylalanine-coated reached higher drug release. Hereby, the results suggest that the functionalization does not play a relevant role in the magnetolipogels as in the magnetogels.

Nonetheless, the concentration and size of the nanoparticle play an important role, as both can induce a diminished passive release owing to the network cavity occupation, and consequently, the triggered release is also hindered (see figure S22 in Supplementary Information). Such effect is highly adequate for drug delivery as the best triggered release is obtained with lower nanoparticle concentration.

Cytotoxicity of the gel components. The magnetic nanoparticles were evaluated for their potential toxicity against the human glioma cell line U373 MG and human neuroblastoma cell line SH-SY5Y. The assays carried out with the manganese ferrite nanoparticles on both cell lines and with the calcium-doped manganese ferrite nanoparticles on the cell line SH-SY5Y are included in Supplementary Information (see figure S23-25). Figure 5B displays the assays of calcium-doped manganese ferrite nanoparticles on the cell line U373 MG.

Overall, no toxicity was detected in the 12.5-100 μg/mL concentration range, except with the manganese ferrites that displayed a slight toxic effect after 48h in the cell line SH-SY5Y. For instance, in the cell line SH-SY5Y, the calcium-doped manganese ferrite nanoparticles did not induce cytotoxicity, and the presence of diphenylalanine even stimulated proliferation at 48h. The same particles also displayed absence of cytotoxic effect at 24h with the cell line U373 MG. However, when compared to the control group (0 μg/mL of nanoparticles), an incremental toxicity is observed at 48 h with the progressive functionalization, mainly in the phenylalanine functionalized particles, but not observed in the particles functionalized with diphenylalanine that display a reduced cytotoxic effect.

The use of phenylalanine has been reported by Nosrati et al. [26] to improve the non-toxic effect compared to bare nanoparticles. Besides, Wu et al. [27] have recently described the use of nanoparticles functionalized with L-phenylalanine to provide specific targeting to the overexpressed human large neutral amino acid transporter SLC7A5 (LAT-1) in cancer cells.

Conclusions

The control and tuneability of drug release have been major objectives of drug delivery systems. For instance, various peptide-based formulations loaded with doxorubicin have been developed as a means to reduce the cardiotoxicity of the chemotherapeutic drug and improve its stability, while seeking improved anti-tumour efficacy [61-64]. Besides the biocompatibility and good tuneability of peptide-based hydrogels, the co-assembly with doxorubicin is of interest owing to the physical interactions between the hydrogel fibres and doxorubicin driving the formation of assemblies that reinforce gel's elastic properties [23,65]. In addition, the electrostatic interactions stablished between doxorubicin and the gel's carboxyl groups is commonly explored as a means for a pH responsive release in weakly acidic conditions. However, these systems can only respond to this pH stimulus, and any change becomes dependent on the balance between doxorubicin and peptide content or a new peptide chemical structure that enables other stimulus (e.g. light).

As the abovementioned challenges can become a hurdle in developing hydrogels with the required properties, we undertook a different approach through the interplay of different composites. First, the use of liposomes demonstrated to be a means to modulate the release of doxorubicin through its encapsulation, which led to a decrease of doxorubicin content available to work as cross-linkers and thus, increasing its release kinetics. Second, the use of nanoparticles functionalized with amine deprotected (di)phenylalanine, which co-assemble with the gel fibres, can suppress the doxorubicin passive release and provide a means for AMF-triggered release. Through the combined use of liposomes and nanoparticles it was possible to advance the modulation of doxorubicin passive release and provide a means for on-demand release through the use of LF-AMF. Besides, the liposomes worked as storage units that can be activated through a temperature trigger to make available more doxorubicin to be released. The developed strategy also provided a means to modulate the gel properties, mainly the gelation kinetics, which besides the nanoparticles was strongly enhanced by the use of PEGylated liposomes.

In this way, the developed strategy provides an alternative to other methods in supramolecular gels that require specific protocols or changes in the chemical structure of the gelator [5,12-19], thus averting undesired effects in the gel's properties and the need to screen a large library of compounds. Also, the library of compounds that can be explored for development of stimuli-responsive gels is widen to other (non)peptide-based gelators, as the presence of both the thermoresponsive liposomes (as storage units) and magnetic nanoparticles provide a mean to achieve an enhanced release under an (low-frequency) alternating magnetic field. Compared to (magnetic) liposomes, the system's design benefits from a higher degree of freedom in the tuneability of the drug release properties as it interplays the effect of different composites. In addition, the diffusion barrier provided by the gel network averts the commonly observed burst and sudden release from the liposomes after a trigger [58,65], which otherwise could cause undesired adverse effects.

Hereby, the fabricated magnetolipogels design promises further developments in the controlled release of other drugs from different peptide-based gels by exploring composites that make use of non-covalent interactions, thus enabling the modulation of known peptide-based gels towards efficacious therapeutic delivery systems.

Author Contributions

S.R.S.V.: conceptualization, investigation, methodology, formal analysis, writing – original draft preparation; E.T.: investigation, formal analysis; C.S.: investigation, formal analysis; L.H.: visualization, validation, formal analysis; C.O.A.: investigation, formal analysis; V.S.A.: visualization, validation, supervision; P.J.G.C.: formal analysis, validation, project administration; P.M.T.F.: methodology, supervision, validation, project administration; V.S.: validation; supervision, writing – review and editing; M.A.C.D.: conceptualization, supervision, writing – review and editing; E.M.S.C.: conceptualization, validation, supervision, writing – review and editing.

Conflicts of interest

There are no conflicts to declare.

Acknowledgements

This work was funded by Ministerio de Economía y Competitividad de España (PID2020-113704RB-I00 and PID2020-119242RB-I00), Xunta de Galicia (Centro Singular de Investigación de Galicia - Accreditation 2019-2022 ED431G 2019/06 and IN607A 2018/5 and project ED431C 2020-06,), and European Union (EU-ERDF Interreg V-A - Spain-Portugal 0245_IBEROS_1_E, 0712_ACUINANO_1_E, and 0624_2IQBIONEURO_6_E, and Interreg Atlantic Area NANOCULTURE 1.102.531), and the European Union H2020-MSCA-RISE-2019 PEPSA-MATE project, and by the Portuguese Foundation for Science and Technology (FCT) in the framework of the Strategic Funding of CF-UM-UP (UIDB/04650/2020), IPC (UID/CTM/50025/2020) and CQUM (UIDB/00686/2020). FCT, FEDER, PORTUGAL2020 and COMPETE2020 are also acknowledged for funding under research projects PTDC/QUI-QFI/28020/2017 (POCI-01-0145-FEDER-028020) and PTDC/QUI-QOR/29015/2017 (POCI-01-0145-FEDER-029015). S.R.S. Veloso acknowledges FCT for a PhD grant (SFRH/BD/144017/2019). Support from MAP-Fis Doctoral Programme is also acknowledged.

References

1 A. Dadwal, A. Baldi and R.K. Narang, *Artif. Cells Nanomed. Biotechnol.*, 2018, **46**, 295-305.
2 V. Trusova, K. Vus, U. Tarabara, O. Zhyniakivska, T. Deligeorgiev and G. Gorbenko, *BioNanoScience*., 2020, **10**, 446-454.
3 A. López-Noriega, C.L. Hatings, B. Ozbakir, K.E. O´Donnell, F.J. O'Brien, G. Storm, W.E. Hennick, G.P. Duffy and E. Ruiz-Hernández, *Adv. Healthc. Mater*., 2014, **3**, 854-859.
4 J.-H. Lee, H. Oh, U. Baxa, S.R. Raghavan and R. Blumenthal, *Biomacromolecules*., 2012, **13**, 3388-3394.
5 S.R.S. Veloso, R.G.D. Andrade and E.M.S. Castanheira, *Adv. Colloid Interface Sci*., 2021, **288**, 102351.
6 M.A. Ramos-Docampo, M. Fernández-Medina, E. Taipaleenmäki, O. Hovorka, V. Salgueiriño, B. Städler, *ACS Nano*, 2019, **13**, 12192-12205.
7 A. Hervault, N. Thanh. *Nanoscale*, 2014, **6**, 11553-11573.
8 T.-K. Nguyen, H.T.T. Duong, R. Selvanayagam, C. Boyer, N. Barraud, *Sci. Rep*., 2015, **5**, 18385.
9 A. Zhang, K. Jung, A. Li, J. Liu, C. Boyer, *Prog. Polym. Sci*., 2019, 2019, **99**, 101164.
10 S.R.S. Veloso, P.J. Jervis, J.F.G. Silva, L. Hilliou, C. Moura, D.M. Pereira, P.J.G. Coutinho, J.A. Martins, E.M.S. Castanheira and P.M.T. Ferreira, *Mater. Sci. Eng. C*, 2021, **122**, 111869.
11 S. Koutsopoulos, *J. Biomed. Mater. Res. A*, 2016, **104**, 1002-1016.
12 S.R.S. Veloso, R.G.D. Andrade, B.C. Ribeiro, A.V.F. Fernandes, A.R.O. Rodrigues, J.A. Martins, P.M.T. Ferreira, P.J.G. Coutinho and E.M.S. Castanheira*, Nanomaterials*, 2020, **10**, 1702.
13 Z. Yang, H. Gu, J. Du, J. Gao, B. Zhang, X. Zhang and B. Xu, *Tetrahedron*, 2007, **63**, 7349-7357.
14 P. Das, S. Yuran, J. Yan, P.S. Lee and M. Reches, *ChemComm*, 2021, **51**, 5432-5435.
15 B.P. Nowak, M. Niehues and B.J. Ravoo, *Soft Matter*, 2021, **17**, 2857-2864.
16 R. Contreras-Montoya, A.B. Bonhome-Espinosa, A. Orte, D. Miguel, J.M. Delgado-López, J.D.G. Duran, J.M. Cuerva, M.T. Lopez-Lopez and L.Á. de Cienfuegos, *Mater. Chem. Front*., 2018, **2**, 686-699.
17 A. Carvalho, J. Gallo, D.M. Pereira, P. Valentão, P.B. Andrade, L. Hilliou, P.M.T. Ferreira, M. Bañobre-López and J.A. Martins, *Nanomaterials*, 2019, **9**, 541.
18 S.R.S. Veloso, J.A. Martins, L. Hilliou, C.O. Amorim, V.S. Amaral, B.G. Almeida, P.J. Jervis, R. Moreira, D.M. Pereira, P.J.G. Coutinho, P.M.T. Ferreira and E.M.S. Castanheira, *J. Mater. Chem. B*, 2020, **8**, 45-64.
19 S.R.S. Veloso, J.F.G. Silva, L. Hilliou, C. Moura, P.J.G. Coutinho, J.A. Martins, M. Testa-Anta, V. Salgueiriño, M.A. Correa-Duarte, P.M.T. Ferreira and E.M.S. Castanheira, *Nanomaterials*, 2021, **11**, 16.
20 M. Kurbasic, C.D. Romano, A.M. Garcia, S. Kralj and S. Marchesan, *Gels*, 2017, **3**, 29.
21 S. Marchesan, L. Waddington, C.D. Easton, F. Kushkaki, K.M. McLean, J.S. Forsythe and P.G. Hartley, *BioNanoScience*, 2013, **3**, 21-29.
22 S.R.S. Veloso, C.A.B. Magalhães, A.R.O. Rodrigues, H. Vilaça, M.-J.R.P. Queiroz, J.A. Martins, P.J.G. Coutinho, P.M.T. Ferreira and E.M.S. Castanheira, *Phys. Chem. Chem. Phys.*, 2019, **20**, 10377-10390.
23 Q. Xue, H. Ren, C. Xu, G. Wang, C. Ren, J. Hao and D. Ding, *Sci. Rep.,* 2015, **5**, 8764.
24 B.D. Cardoso, A.R.O. Rodrigues, B.G. Almeida, C.O. Amorim, V.S. Amaral, E.M.S. Castanheira and P.J.G. Coutinho, *Int. J. Mol. Sci*., 2020, **21**, 3641.
25 P.Y. Reyes-Rodríguez, D.A. Cortés-Hernández, C.A. Ávila-Orta, J. Sánchez, M. Andrade-Guel, A. Herrera-Guerrero, C. Cabello-Alvarado and V.H. Ramos-Martínez, *J. Magn. Magn. Mater.*, 2021, **521**, 167518–167527.
26 H. Nosrati, H. Hamzehei, S. Afroogh, S.F. Ashabi, E. Attari and H.K. Manjili, *Drug Res.*, 2019, **69**, 277-283.
27 Z. Wu, H.K. Lim, S.J. Tan, A. Gautam, H.W. Hou, K.W. Ng, N.S. Tan and C.Y. Tay, *Small*, 2020, **16**, e2003757.
28 M. Häring, J. Schiller, J. Mayr, S. Grijalvo, R. Eritja, D.D. Díaz, *Gels*, 2015, **1**, 135-161.
29 P. Ferreira, L. Monteiro, G. Pereira, L. Ribeiro, J. Sacramento and L. Silva, *Eur. J. Org. Chem.*, 2007, **2007**, 5934-5949.

30 H. Vilaça, G. Pereira, T. Castro, B. Hermenegildo, J. Shi, T. Faria, N. Micaêlo, R. Brito, B. Xu, E. Castanheira, J. Martins and P. Ferreira, J. Mater. Chem. B, 2015, 3, 6355-6367.

31 B. Szała and A. Molski, *Biomolecules,* 2020, **10**, 1362.

32 J. Vymětal and J. Vondrášek, *J. Phys. Chem. A*, 2011, **115**, 11455-11465.

33 A. Fuentes-Caparrós, F. de Paula Gómez-Franco, B. Dietrich, C. Wilson, C. Brasnett, A. Seddon and D.J. Adams, *Nanoscale*, 2019, **11**, 3275-3280.

34 A. Morris, M. Watzky and R. Finke, *Biochim. Biophys. Acta, Proteins Proteomics*, 2009, **1794**, 375-397.

35 C. Poojari, N. Wilkosz, R. Lira, R. Dimova, P. Jurkiewicz, R. Petka, M. Kepczynski and T. Róg, *Chem. Phys. Lipids*, 2019, **223**, 104784.

36 M. Ullrich, J. Hanuš, J. Dohnal and F. Štěpánek, *J. Colloid Interface Sci.*, 2013, **394**, 380-385.

37 M. Testa-Anta, M.A. Ramos-Docampo, M. Comesaña-Hermo, B. Rivas-Murias and V. Salgueiriño, *Nanoscale Adv.*, 2019, **1**, 2086.

38 F. Nekvapil, A. Bunge, T. Radu, S.C. Pinzaru and R. Turcu, *J. Raman Spectrosc.,* 2020, **51**, 959-968.

39 G. Zhu, X. Zhu, Q. Fan and X. Wan, *Spectrochim. Acta A*, 2011, **78**, 1187-1195.

40 B. Hernández, F. Pflüger, S.G. Kruglik and M. Ghomi, *J. Raman Spectrosc.*, 2013, **44**, 827-833.

41 M. Hiraoui, M. Guendouz, N. Lorrain, A. Moadhen, L. Haji and M. Oueslati, *Mater. Chem. Phys.*, 2011, **128**, 151-156.

42 I.H. Boyaci, H.T. Temiz, H.E. Geniş, E.A. Soykut, N.N. Yazgan, B. Güven, R.S. Uysal, A.G. Bozkurt, K. İlaslan, O. Torun and F.C.D. Şeker, *RSC Adv.*, 2015, **5**, 56606-56624.

43 H. Zhang, H.-X. He, J. Wang, T. Mu and Z.-F. Liu, *Appl. Phys. A*, 1998, **66**, S269-S271.

44 I. Obaidat, B. Issa and Y. Haik, *Nanomaterials,* 2015, **5**, 63-89.

45 L.C. Branquinho, M.S. Carrião, A.S. Costa, N. Zufelato, M.H. Sousa, R. Miotto, R. Ivkov and A.F. Bakuzis, *Sci. Rep.*, 2013, **3**, 2887.

46 S. Nemec, S. Kralj, C. Wilhelm, A. Abou-Hassan, M.-P. Rols and J. Kolosnjaj-Tabi, *Appl. Sci.*, 2020, **10**, 7322.

47 A.B. Bonhome-Espinosa, F. Campos, I.A. Rodriguez, V. Carriel, J.A. Marins, A. Zubarev, J.D.G. Duran, M.T. Lopez-Lopez, *Soft Matter*, 2017, **13**, 2928-2941.

48 K. Hyun, M. Wilhelm, C. Klein, K. Cho, J. Nam, K. Ahn, S. Lee, R. Ewoldt and G. McKinley, *Prog. Polym. Sci.*, 2011, **36**, 1697-1753.

49 J. John, D. Ray, V.K. Aswal, A.P. Deshpande and S. Varughese, *Soft Matter*, 2019, **15**, 6852-6866.

50 J. Liu, H. Zheng, P. Poh, H. Machens and A. Schilling, *Int. J. Mol. Sci.*, 2015, **16**, 15997-16016.

51 C. Amorim, S.R.S. Veloso, E.M.S. Castanheira, L. Hilliou, R.B. Pereira, D.M. Pereira, J.A. Martins, P.J. Jervis and P.M.T. Ferreira, *Gels*, 2021, **7**, 52.

52 H. Vilaça, A. Hortelão, E. Castanheira, M. Queiroz, L. Hilliou, I. Hamley, J.A. Martins and P.M.T. Ferreira, *Biomacromolecules*, 2015, **16**, 3562-3573.

53 R. Orbach, L. Adler-Abramovich, S. Zigerson, I. Mironi-Harpaz, D. Seliktar and E. Gazit, *Biomacromolecules*, 2009, **10**, 2646-2651.

54 R. Otero-Lorenzo, E. Fantechi, C. Sangregorio, V. Salgueiriño, *Chem. Eur. J*, 2016, **22**, 6666-6675.

55 P.L. Ritger and N.A. Peppas, *J. Control. Release*, 1987, **5**, 23–36.

56 S. Dash, P.N. Murthy, L. Nath and P. Chowdhury, *Acta Pol. Pharm.*, 2010, **67**, 217-223.

57 J. Ghitman, R. Stan, A. Ghebaur, S. Cecoltan, E. Vasile and H. Iovu, *Polymers*, 2018, **10**, 579.

58 Z.S. Al-Ahmady, W.T. Al-Jamal, J.V. Bossche, T.T. Bui, A.F. Drake, A.J. Mason and K. Kostarelos, *ACS Nano*, 2012, **6**, 9335-9346.

59 K.Y. Vlasova, S.C. Vanzarakshaeva, M.M. Veselov, I.M. Le-Deygen, A.V. Petrunin, A.N. Prusov, A.B. Shuklinov, Y.I. Golovin, A.V. Kabanov and N.L. Klyachko, *Mosc. Univ. Chem. Bull.*, 2020, **75**, 232-237.

60 S. Nappini, M. Bonini, F. Ridi and P. Baglioni, *Soft Matter*, 2011, **7**, 4801-4811.

61 E. Gallo, C. Diaferia, E. Rosa, G. Smaldone, G. Morelli and A. Accardo, *Int. J. Nanomed.*, 2021, **16**, 1617-1630.

62 L. Mei, K. Xu, Z. Zhai, S. He, T.Zhu and W. Zhong, *Org. Biomol. Chem.*, 2019, **17**, 3853-3860.

63 S. Li, X. Chen, H. Chen, J. Peng and X. Yang, *Molecules*, 2020, **25**, 484.

64 C. Diaferia, E. Rosa, A. Accardo and G. Morelli, *Pep. Sci.*, 2021, e3301. https://doi.org/10.1002/psc.3301

65 W. Lin, X. Xie, Y. Yang, X. Fu, H. Liu, Y. Yang, J. Deng, *Drug Delivery*, 2016, 23, 3436-3443.